Characterization and Design of a PLC Coupling System Based on Capacitive Divider Embedded in MV Cable Head

Giovanni Artale, *Member, IEEE*, Antonio Cataliotti, *Member, IEEE*, Valentina Cosentino, *Member, IEEE*, Dario Di Cara, *Member, IEEE*, Vito Ditta, Salvatore Guaiana, Nicola Panzavecchia, and Giovanni Tinè, *Member, IEEE*

***Abstract*—Power line communication (PLC) technology is exploited worldwide for automatic meter reading on low-voltage networks. On the contrary, it is not used at medium voltage (MV) level, where it requires dedicated and costly PLC couplers. To face this issue, in previous works the authors investigated the possibility of reducing costs by coupling the signal by means of elements already installed in MV networks. A patented solution was based on the exploitation of capacitive dividers of voltage detective systems (VDSs) normally installed in MV switchgears of distribution network's substations. This paper investigates the use of capacitive dividers embedded in commercial separable connector of MV cables heads, instead. In comparison with VDSs, cable heads voltage dividers have different characteristics; thus an ad-hoc characterization and design of PLC coupling system is presented and discussed. Firstly, impedance measurements are performed to characterize cable heads behavior in the frequency range of interest. An equivalent circuit model is obtained and used to design an electronic interface card for signal coupling. Simulations and experimental tests are performed in FCC above CENELEC frequency band, to analyze channel frequency response and transmission performances, in terms of success rate and SNR. The results testify the proposed coupling solution feasibility.**

***Index Terms*—Power system communication, frequency response, smart grids, power line communications, distributed measurement systems.**

Manuscript received 10 July 2023; revised 13 December 2023; accepted 7 February 2024. Date of publication 15 February 2024; date of current version 23 May 2024. This work was supported by Ricerca di Sistema Nel Settore Elettrico Three-Year Plan 2022–2024, through Projects Progetto 2.1 - Progetto Integrato Cyber Security Dei Sistemi Energetici, under Grant CUP: B53C22008530001 and Program IEV CT Italie Tunisie 2014-2020, under Project IS_2.1_131, Solutions Innovantes Pour L'intégration Des Énergies Renouvelables Sur le Réseau Électrique Tunisien", Project acronym: SInERT, under Grant CUP: B74I19001040006 and Grant B74I18014130002. Paper no. TPWRD-00971-2023. *(Corresponding author: Giovanni Artale.)*

Giovanni Artale, Antonio Cataliotti, Valentina Cosentino, and Vito Ditta are with the Department of Engineering, Università di Palermo, 90133 Palermo, Italy (e-mail: giovanni.artale@unipa.it; antonio.cataliotti@unipa.it; valentina.cosentino@unipa.it; vito.ditta@unipa.it).

Dario Di Cara, Salvatore Guaiana, Nicola Panzavecchia, and Giovanni Tinè are with the Institute of Marine Engineering (INM), National Research Council (CNR), 16149 Palermo, Italy (e-mail: dario.dicara@cnr.it; guaiana.salvatore@inwind.it; nicola.panzavecchia@cnr.it; giovanni.tine@cnr.it).

Color versions of one or more figures in this article are available at https://doi.org/10.1109/TPWRD.2024.3366419.

Digital Object Identifier 10.1109/TPWRD.2024.3366419

I. Introduction

ACQUIRING measurements in different points of medium voltage (MV) networks is a need for Distribution System Operators (DSOs) all around the world. Apart from typical measurements of active and reactive powers for billing purposes, advanced smart grids monitoring and control functions require the knowledge of many other electrical quantities (i.e., voltages, currents, power quality quantities, and so on) in different points of the network, such as secondary substations, MV users' substations or distributed generators. To this aim, the number of measurement instruments and transducers installed in the network and their accuracy requirements are steadily increasing [1], [2], [3], [4]. Furthermore, the growing diffusion of distributed generation entails numerous problems concerning the possibility of energy flows inversion, rapid voltage variations, short-circuit currents increase, islanding occurrence and so on. Thus, new monitoring and control equipment are needed to guarantee a reliable management and protection of electrical networks [5]. All these applications require an information exchange between DSOs and field measurement instruments and control devices. Thus, a communication infrastructure is an essential requirement for developing smart grids.

Different wireless communication systems can be used for data transmission between DSOs and prosumers such as GSM, GPRS, WiMAX, LTE, etc. [6]. The fundamental disadvantages of all these systems are their reliance on a communication provider and their low reliability, particularly in bad weather conditions. On the other hand, an ad-hoc wired infrastructure (e.g., in fiber optic) would be too expensive for reaching every user in the case of rural or out of town areas or in general in areas with low population density. In this viewpoint, PLC technology may be a viable solution because the communication lines are already present (i.e., the power lines) and there are no service costs [7]. Some applications, such as automatic meter reading and advanced metering infrastructure, are already supported by PLCs in low voltage (LV) networks [8], [9], [10], [11]. On the other hand, PLCs use at medium voltage (MV) level is less used, because it entails different issues, concerning both the grid characteristics and the signal coupling. In fact, MV networks and secondary substations can have different configurations [12], [13], [14]. Thus, to couple a signal on MV lines, several aspects

must be considered, such as physical coupling typology, voltage and impedance levels, frequency bandwidths, propagation modes, numbers of connections, and so on.

PLC signal coupling can be capacitive, inductive, resistive or it can be made by an antenna [15], [16], [17], [18], [19], [20], [21], [22]. In very brief, a PLC coupler should offer a low impedance path for high frequency PLC signal and a high impedance at power systems frequencies to prevent that mains voltage is applied to the transceiver.

The simplicity, affordability, and straightforward installation and operation of antennas made them the initial choice for connecting PLC transceivers to power lines. However, the inefficient loss of power caused this kind of coupling to be discontinued. On the other hand, recent research interest in hybrid wireless-PLC communication systems could give a new boost to their application [23]. Capacitive coupling involves the connection of one or more capacitors to the MV power line. Capacitive couplers are a good choice when the active conductor of a power line is easily accessible, as in the case of overhead power lines. On the other hand, some solutions were presented also for capacitive coupling in MV cable lines [24]. In both overhead and cable power lines cases, the installation of a capacitive coupler requires the cost of the coupler itself and the temporary disconnection of the mains voltage for its installation; in the case of cable power lines, the modification of the MV switchboard is needed too. On the other hand, this typology of coupling is very reliable, and it has low losses. In the case of MV cables, inductive couplers can be much easier clamped on the power line [25]. The electromagnetic field generated by the current flowing in the coil loads inductively the signal into the MV conductor; this causes insertion losses and phase and linearity problems, depending on the toroidal core material. In the case of a resistive coupler, a voltage divider, a bandpass filter, and an amplifier are used, instead [26]. For isolation issues, this type of coupling is more suitable for LV networks.

All the aforesaid coupling solutions have high costs for signal couplers installation. In fact, MV couplers should be installed both in primary substation (at MV busbars) and in all MV/LV secondary substations. This involves not only the costs of the equipment, but also those of MV switchboards modifications and the energy interruptions for their installation. To face these issues, the authors have patented a new coupling system, which allows injecting and receiving the PLC signal by means of the capacitive divider embedded in the voltage detective system (VDS), according to IEC 61243-1 [16], installed in the MV switchgears of distribution network's substations [27]. This reduces the installation cost and avoids electrical service interruptions. A suitable electronic interface card was designed and developed to transmit and to receive narrowband n-PSK PLC signals in CENELEC band [28], [29]. In [31] the innovative coupling system was updated to work also with Orthogonal Frequency-Division Multiplexing (OFDM) modulated signals in G3-FCC band, from 154.6875 to 487.5 kHz.

Starting from this first proposal, in this paper an alternative low cost MV coupling solution is presented, which can allow exploiting a different electrical element installed in secondary substations, when VDS is not available. In particular, the work is focused on the characterization and design of a MV PLC coupler based on the use of capacitive divider embedded in commercial cable separable connector (SC) of MV cables heads, which are employed in distribution network substations to connect the MV cable head to the MV switchboard. This element embeds a capacitive divider to detect the mains voltage presence in the MV network. In comparison with the VDS, the SC voltage divider has different standard features [30]; thus, to enable the PLC signal transmission and reception, an ad-hoc design for the coupling circuit is herein presented and discussed.

The paper is organized as follows. Firstly, the SC characterization in the frequency range of interest is described in Section II. Secondly, the design and the development of the SC-based coupler prototype is reported in Section III. Finally, laboratory experimental results are presented to verify the new prototype performances.

II. Characterization of Capacitive Divider Embedded in Commercial Cable Separable Connector (SC) of MV Cables Heads

As mentioned in the introduction, the idea of the work is to use the intrinsic capacitance embedded in the SC of MV cable head as coupler for PLC signals.

In general, the SC capacitive divider is made of a series of two capacitances, i.e., the first one is connected to the MV cable and the second one has two available terminals for voltage detection. The second of these terminals can be connected to earth. In this case, the cable SC behavior would be the same of VDS, thus the coupling interface card presented in [28] could be still used for PLC signal injection. However, as shown in the following, preliminary test results showed that the use of this method does not give good transmission results when the cable SC is directly connected to earth.

Thus, a different solution is presented in this paper, which is based on the SC connection to earth by means of an inductance. An ad-hoc interface card was developed for such a solution. As shown in the following, this second design significantly increased the transmission performances. To properly design the coupling circuit for enabling the PLC signal transmission and reception, the knowledge of the SC characteristics in the frequency range of interest are needed. Thus, an experimental characterization has been carried out, by measuring the input and output impedances seen from each available couple of terminals.

The SC used for the characterization is a commercial fully shielded molded body in vulcanized Ethylene-Propylene Diene Monomer (EPDM) insulating rubber. It is suitable for the connection of MV cables to equipment such as power transformers or actuating switches, which embed pass-through sockets for voltage-free separation. The whole connection system is shown in Fig. 1, in fact it is the combination of a SC on the cable and a bushing socket at the transformer side. The SC is inserted into the internal cone by means of a pass-through insulator. It is locked to it by means of special screws on the respective flanges. The line must be de-energized when inserting or removing the connector. In the SC termination, the absence of MV voltage can be checked by using the capacitive detector integrated in the connector

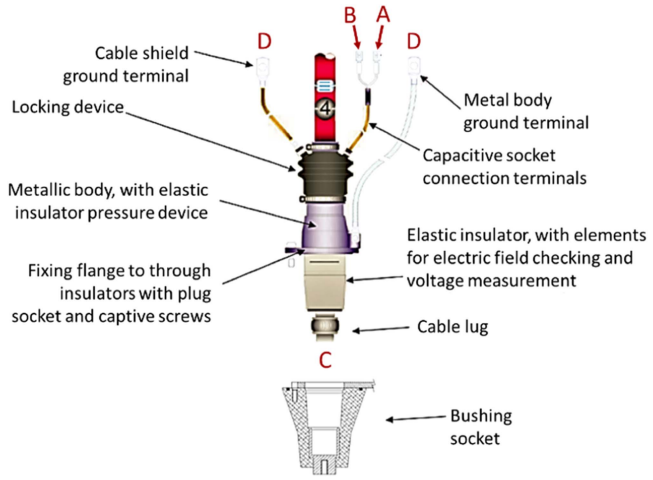

Fig. 1. Scheme of commercial SC used for PLC tests.

and / or in the bushing. The SC terminals are highlighted in Fig. 1(a) and (b) are the capacitive socket terminals used to detect the voltage presence; C is the core of the medium voltage cable; D are the ground terminals for cable shield and metallic body.

The study presented in this paper was aimed at verifying the possibility of transmitting PLC signals through these terminals. To do this, firstly the SC was characterized by measuring the frequency response in the PLC frequency range of interest. In particular, the FCC above CENELEC frequency band was considered, according to IEEE STD 1901.2-2013, i.e., from 154.6875 kHz to 487.500 kHz. The SC was characterized in the whole aforesaid frequency range. In fact, according to IEEE Std 1901.2-2013, the OFDM signal can have a frequency band corresponding to the whole frequency range, in the case of 72 sub-carriers, or to a frequency band of 160 kHz or 80 kHz, when the OFDM signal is composed of 36 sub-carriers or 18 sub-carriers, respectively.

The characterization was carried out by using a Keysight ENA E5080A vector network analyzer (VNA) [32]. This instrument was used to measure the impedance seen from the different available terminals, thus obtaining an equivalent circuit of the plug-in connector. The VNA has been set in the range 50 - 500 kHz with a step of 1 kHz and a RBW equal to 1 kHz. A full one-port manual calibration was performed before each series of measurements, by using a Keysight 85032F calibration kit [33]. The connectors of the calibration kit have the following characteristics that is phase uncertainty of open-circuit connector impedance smaller than 1.0°; phase uncertainty of short-circuit connector impedance smaller than 1.0°; return loss of match-circuit connector higher than 48 dB. All these parameters are defined in the frequency range 0–4 GHz. After system errors correction, the reflection measurements accuracies were 0.1 dB and 1°.

Three impedance measurements were carried out, between different SC terminals, as named in Fig. 1:

- Impedance between core and shield (C–D impedance);
- Impedance between capacitive socket terminals (A–B impedance);
- Impedance between core and capacitive socket terminal (A–C impedance).

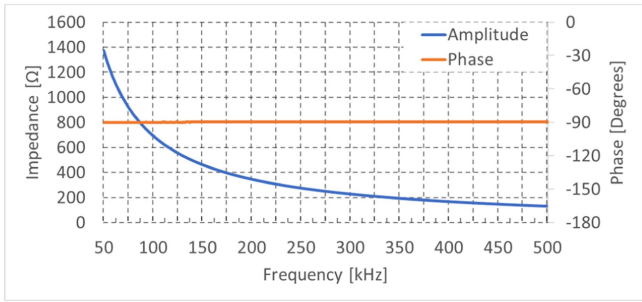

Fig. 2. Measured amplitude and phase of impedance between C–D terminals.

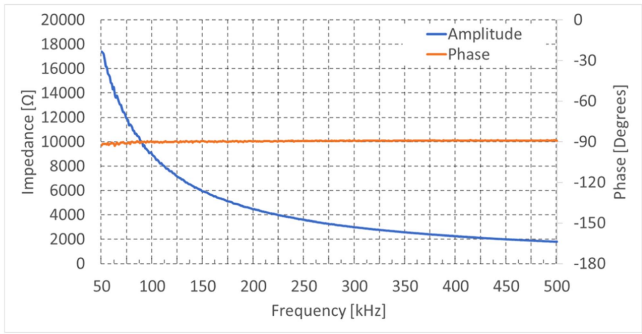

Fig. 3. Measured amplitude and phase of impedance between A–B terminals.

To measure the C–D impedance between shield and core, A and B connectors were left open; D terminals were connected to earth. The graphs of measured module and phase of C–D impedance are shown in Fig. 2. The measured phase and amplitude variations with frequency show a capacitive behavior in the frequency range of interest (154.6875 - 487.500 kHz).

To measure the impedance between the capacitive socket terminals, A and B connectors were connected to the VNA measurement channel, while C and D terminations were left open. Terminal B was connected to the measurement instrument ground. Fig. 3 show the measured amplitude and phase of A–B impedance, respectively. Also in this case, the measured impedance has a capacitive behavior, since the phase value is constant and equal to −90° in the whole considered frequency range.

As regards the A–C impedance measurement, it should be noted that the plug-in connector has a ring of insulating material concentric with the MV cable core. It separates the cable conductor from an external metal ring. This last is used to derive a voltage proportional to the mains voltage, thus identifying the network presence. According to Fig. 1, to measure the impedance between this metal ring and the cable core connectors, B and D terminals have been left open and the impedance was measured between A and C terminals. Amplitude and phase of the measured A–C impedance are shown in Fig. 4. Also in this case a capacitive behavior was found.

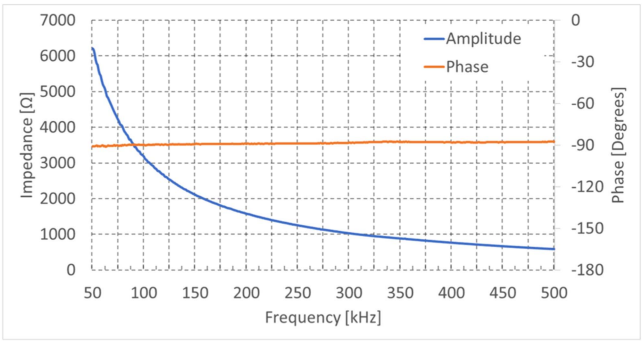

Fig. 4. Measured amplitude and phase of impedance between A–C terminals.

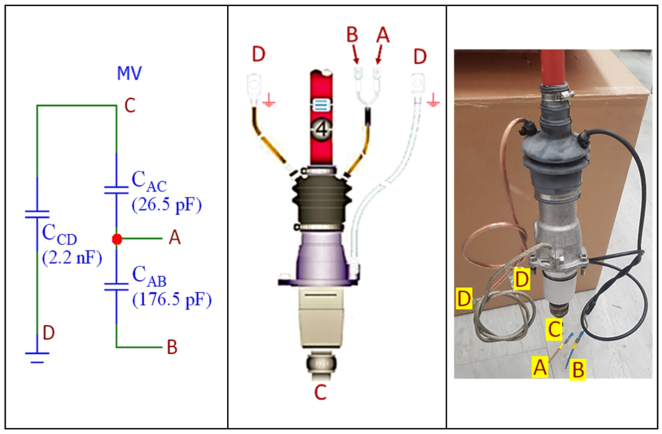

Fig. 5. Equipment under test and equivalent wiring diagram of separable connector (on the left: SC equivalent circuit; in the center: SC scheme; on the right: photo of the SC under test).

III. SC-based Coupling System Design and Development.

A. Experimental and Modeling Approach for SC-based Coupling Design and Development

The characterization study results showed that all the impedance measured between the different SC terminals have a predominantly capacitive behavior. Thus, the equivalent circuit diagram of the SC system can be drawn as shown in Fig. 5.

The SC-based coupling solution makes use of SC A and B terminals to inject the PLC signal. According to the equivalent circuit of Fig. 5, the impedance seen between these two terminals behaves as a series of capacitances. Since B terminal is originally floating, it can be connected to earth or not. As mentioned in Section II, when B is connected to earth, a VDS-like system is obtained; however, in comparison with the VDS-based solutions the value of impedance to ground at PLC signal frequency is too low, thus the signal transmission does not provide effective results. In the proposed solution, an inductance (named L_{BD}) is connected between B terminal and earth, instead. This inductance has the function of increasing the total impedance to earth at PLC signal frequency, while it shows a low impedance at mains frequency. In fact, $|Z_L| = 2\pi f L$, thus the impedance offered at mains frequency (50 Hz) is very low, while a high impedance is obtained at PLC signal frequency (higher than 150 kHz). The values of capacitances C_{AC} and C_{AB} cannot be predicted accurately; therefore it is not possible to establish a priori the amplitude of the signal transmitted on one side and received on the other one. As shown in [28], even in the case of VDS it is impossible to know in advance the parasitic capacitance; in fact, the circuit can be represented by the series of the MV divider capacitance and the LV circuit equivalent capacitance, which includes also parasitic capacitances that are not knowable in advance.

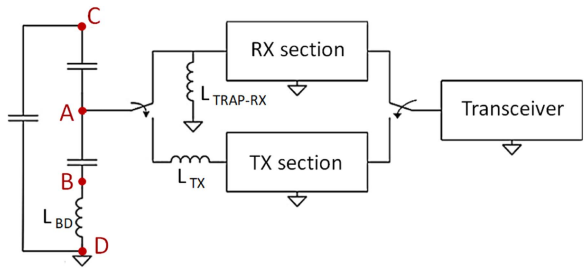

Fig. 6. System block diagram.

The circuit shown in Fig. 5 refers only to the SC. The impedance shown by the cable (when the connection is made for signal transmission or reception) should be added to this schematic. However, the prototype of the proposed coupling system is based on researching the resonance condition between the variable inductance and the overall capacitance of the entire transmission/reception channel. Thus, it is unnecessary to model the cable capacitance at this stage. In fact, as shown in the following, once the prototype is connected to terminals A–B, it is possible to achieve the resonance condition by properly tuning the inductances both in RX and TX mode.

The SC is based on a principle similar to that of the VDS, except that in the VDS one capacitance terminal is ground-connected, while in the SC such terminal is floating (B terminal).

For both TX and RX sections, the main electrical requirement is to show the PLC signal a high impedance to ground and a low impedance to the transceiver. To this aim, two circuits were designed, one for transmission and one for reception. They were both included in an interface electronic board, which is meant to be connected between the transceiver and the SC terminals.

The system block diagram is shown in Fig. 6. Two switches are used to select the circuit for TX or RX mode. The first switch is connected to A terminal, and the second switch is connected to the transceiver. The switches commutate the state of both the prototype and the transceiver, to receive or transmit information. The impedance level to be shown between A and D changes depending on the transceiver state (RX or TX). In TX, the circuit shows low impedance to create a series resonance, while in RX a high impedance is shown due to the creation of a parallel resonant circuit. In the following, the two block schemes are analyzed in detail.

B. Transmission Circuit Scheme

The transmission (TX) circuit scheme is shown in Fig. 7. The PLC signal injected by the transceiver is amplified by a TX section and injected into the SC A terminal. To maximize the voltage signal amplitude between A and B, two inductances are

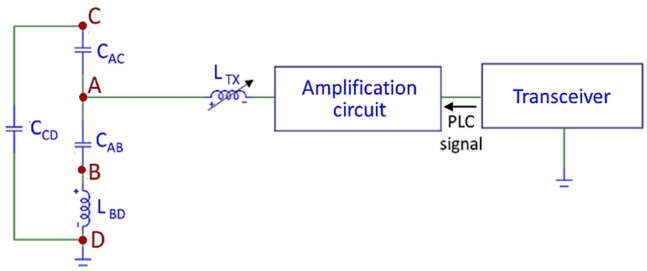

Fig. 7. Transmission section scheme.

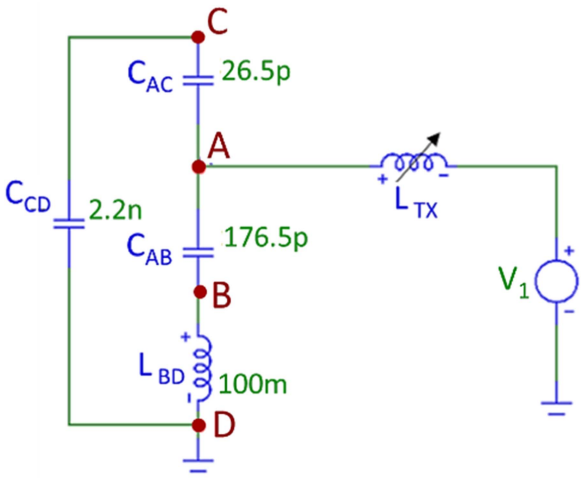

Fig. 8. Wiring diagram used for simulation of transmission section.

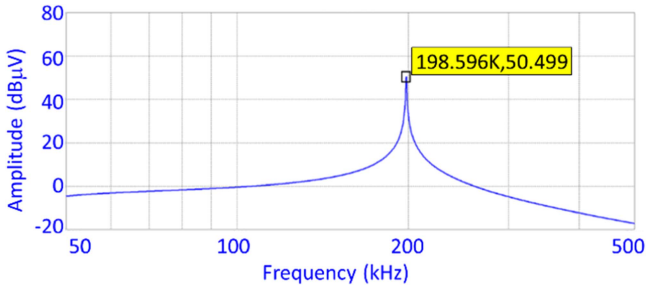

Fig. 9. Frequency response of transmission section (obtained between A–D terminals).

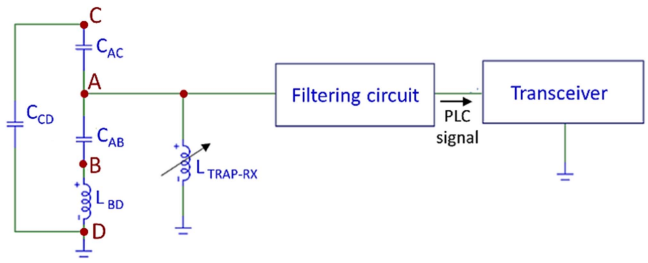

Fig. 10. Reception section scheme.

connected to the TX section output. The first inductance, L_{BD}, is connected between terminal B and ground. It is used to increase the impedance to earth at signal frequency. A second tunable L_{TX} inductance was designed to create a resonant circuit at PLC signal frequency with the equivalent capacitance seen between A terminal and earth. Thanks to the tuning of such series resonant circuit, a high voltage is obtained at A terminal.

Thanks to the combined use of L_{BD} and L_{TX}, the largest part of the PLC signal is injected into the MV line, while a reduced part is short-circuited to earth. More in detail, the inductance value is tuned to obtain a resonance in correspondence to the center frequency of the considered tone mask band. Thus, the signal tone mask can be easily changed by tuning the inductance to a different value.

Besides the resonant circuit, an amplification circuit is also included into TX section. It consists of an amplifier and a transistors push-pull circuit, which allows increasing the injected current required by the resonant circuit. Specifically, a BJT push-pull driven by an op-amp with a gain of 3 was used for the tests presented in the following.

To verify the correct behavior of the designed transmission circuit, simulations were performed at different frequencies. The electric equivalent scheme for TX circuit simulation is shown in Fig. 8. The simulation was focused on the coupling circuit; thus the amplification circuit and the transceiver are schematized with a voltage generator V1. C_{AB}, C_{AC} and C_{CD} values are those measured using the procedures described in Section II. L_{BD} value was set to 100 mH; L_{TX} value was tuned to maximize voltage amplitude as close as possible to the center frequency of one of the sub-bands. In detail, a 33mH inductance was set to obtain the resonance condition. V1 generates a 1 V sinusoidal sweep with variable frequency from 50 kHz to 500 kHz. As an example, Fig. 9 shows the frequency response results (obtained between A-D terminals) in the case of tone mask between 154.6875 and 234.375 kHz with center frequency f = 194 kHz. Resonance frequency is at about 198 kHz having a gain of about 50.5dB.

C. Reception Circuit Scheme

The block scheme of reception (RX) circuit is shown in Fig. 10. This circuit is designed for amplifying and filtering the modulated signal coming from MV, so to increase its voltage level and the corresponding SNR; the RX output signal will be demodulated by the transceiver.

L_{BD} and C_{AB} have fixed values. They create a series resonant circuit outside the frequency range of interest. On the other hand, a parallel resonant group is obtained by means of C_{AB}+L_{BD} and the tunable inductance L_{TRAPRX}. In detail, L_{TRAPRX} value is tuned to obtain a parallel resonant circuit at tone mask center frequency. The parallel resonant circuit has a very high impedance at signal frequency, thus resulting in high voltage and SNR at signal frequency which make easier the signal demodulation. By varying L_{TRAPRX}, the resonant frequency can be moved to be as close as possible to the desired tone mask center frequency. Also in this case, the resonance condition was obtained with a 33 mH inductance.

The RX coupling circuit was tested using the electrical simulation scheme shown in Fig. 11. The frequency response was obtained with a sweep signal injected between C terminal and earth. As an example, Fig. 12 shows the frequency response

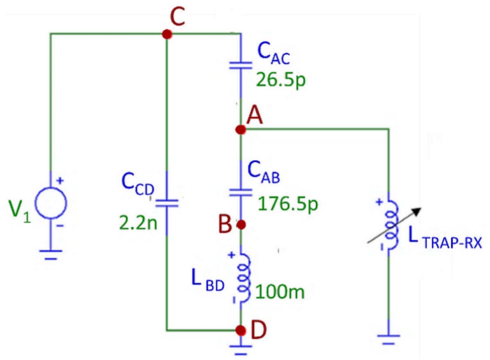

Fig. 11. Wiring diagram used for simulation of reception section (obtained between A–D terminals).

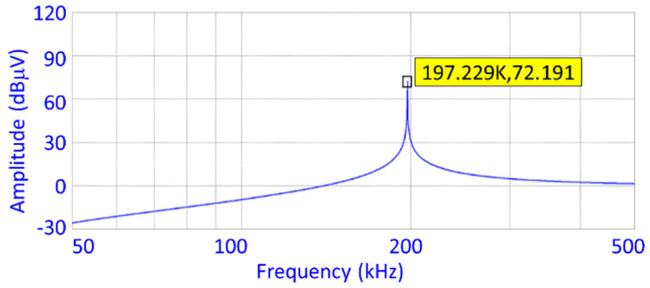

Fig. 12. Frequency response of reception section.

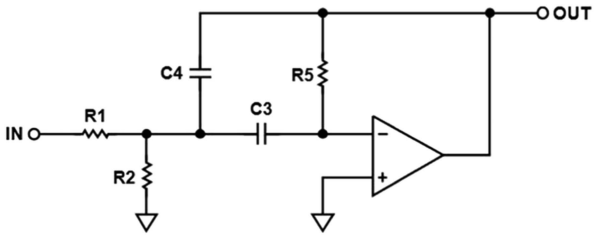

Fig. 13. Schematic of a multiple feedback second-order active filter.

results (obtained between A-D terminals) in the case of tone mask between 154.6875 and 234.375 kHz with center frequency f = 194 kHz. Thanks to resonance, signal is increased of about 72 dB, with respect to other frequencies. However, to further minimize the noise, a filtering circuit was designed and added between SC-A terminal and the transceiver, as shown in Fig. 10.

The filtering stage consists of a buffer for impedance decoupling, a multiple feedback active filtering section, an adder and two series VCVS (Voltage Controlled Voltage Source) active filters (Fig. 13). The complete RX section with a block diagram of the filtering circuit is shown in Fig. 14.

As mentioned before, the signal at A terminal can be low and very noisy, so it is important to properly filter and amplify it. The performances of the parallel multiple feedback active filters were investigated in [29]. It was shown that they can eliminate external band noise and increase the signal amplitude to have a good equalization. In detail, three parallel multiple feedback active filters with different gains and center frequencies were used; they allow covering all 18 or 36 sub-carriers of each tone mask, so to guarantee a high success rate. The three filters have tunable parameters which allow changing the tone mask. This filtering

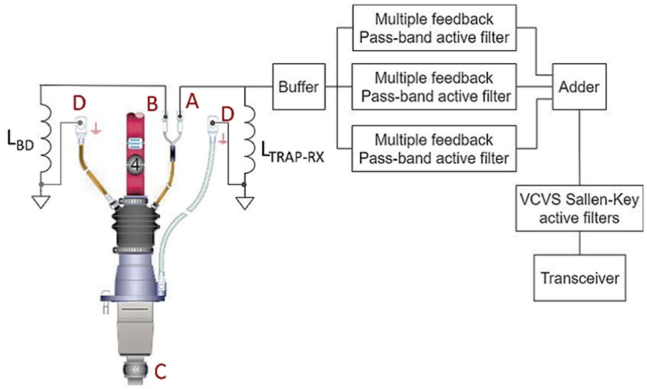

Fig. 14. Block scheme of RX section.

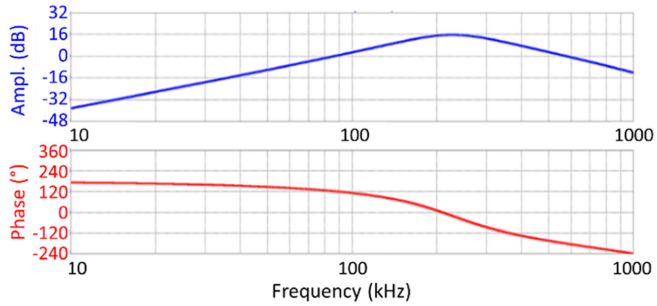

Fig. 15. Amplitude (blue) and phase (red) plots of Sallen-Key active filters.

section was suitable in the case of signal coupling through VDS. On the other hand, in the case of the SC analyzed in this paper, the obtained SNR was worse than in the case of VDS, thus a further filtering solution was designed and added. In detail, a Sallen-Key active second order VCVS filter was designed and included in the RX section. It allows both amplifying and further filtering the signal from external frequencies.

The VCVS response is shown in Fig. 15. Two series band pass filters were realized with very close central frequencies. The filters have sufficient side bands attenuation to remove high frequency noises. Moreover, a higher gain was obtained at lower frequencies. Ultra-low noise operational amplifiers were used in the circuit simulation and then included the electronic board prototype. Micro-Cap 12 was used to perform the circuit simulation. Fig. 15 shows filters frequency response obtained in simulation between 10 kHz and 1 MHz. Signal is amplified between 150 kHz and 400 kHz with a slope of 40 dB / decade. The whole reception section was also simulated in Micro-Cap environment. As an example, the simulation for the first tone mask between 154 and 234 kHz with center frequency at 194 kHz is shown in Fig. 16, i.e., the multiple feedback pass-band filter parameters were tuned to obtain a flat frequency response at transceiver input.

D. SC-based Coupling System Wiring in Real environment.

The complete wiring diagram, including the power electrical system, is shown in Fig. 17. The SC terminal C is connected to the MV cable, while through connectors A and B is connected the prototype for signal injection to the MV line. The interface

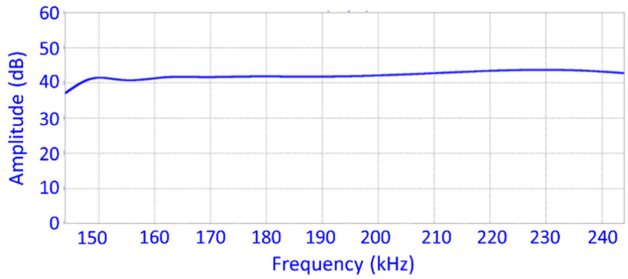

Fig. 16. RX section frequency response.

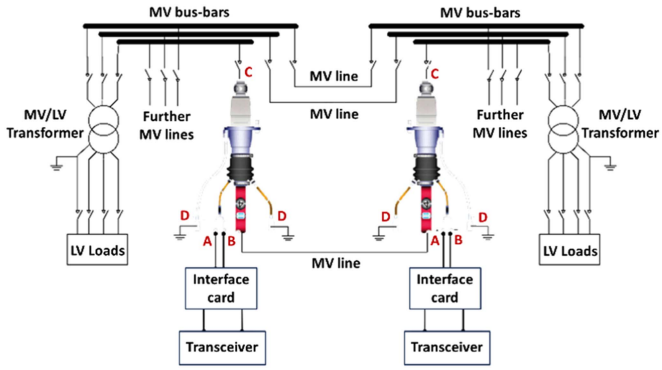

Fig. 17. Complete wiring diagram including MV line and secondary substation switchboard. The Interface Cards embed RX and TX circuits for PLC signal coupling.

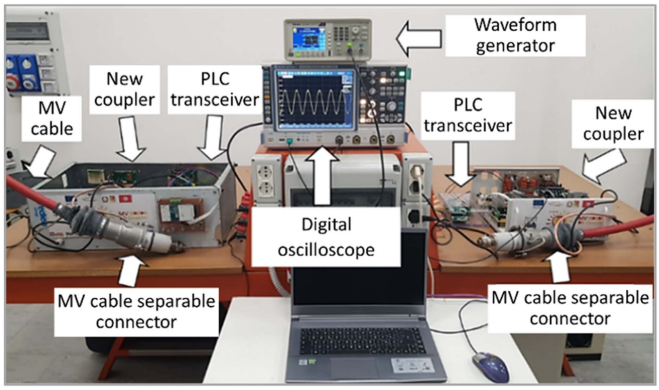

Fig. 18. Test bench used in laboratory.

cards embed the developed coupling circuits (both RX and TX sections) described in the previous sections. The transceivers connected to the interface cards provide for modulation (in transmission phase) and demodulation (in reception phase) of the signal to be injected on the MV.

The scheme is conceptually similar to that employed in [29] for on-field demonstration of the VDS solution. Generally speaking, the effects of power line cable impedance result in both attenuation and phase shifting of the signal along the path. Both are highly dependent on the length and characteristics of the power line connecting the two points from which communication is made. As regards this, practical on-field tests on the VDS system were presented in [29]. These tests were carried out between two secondary substations connected by a

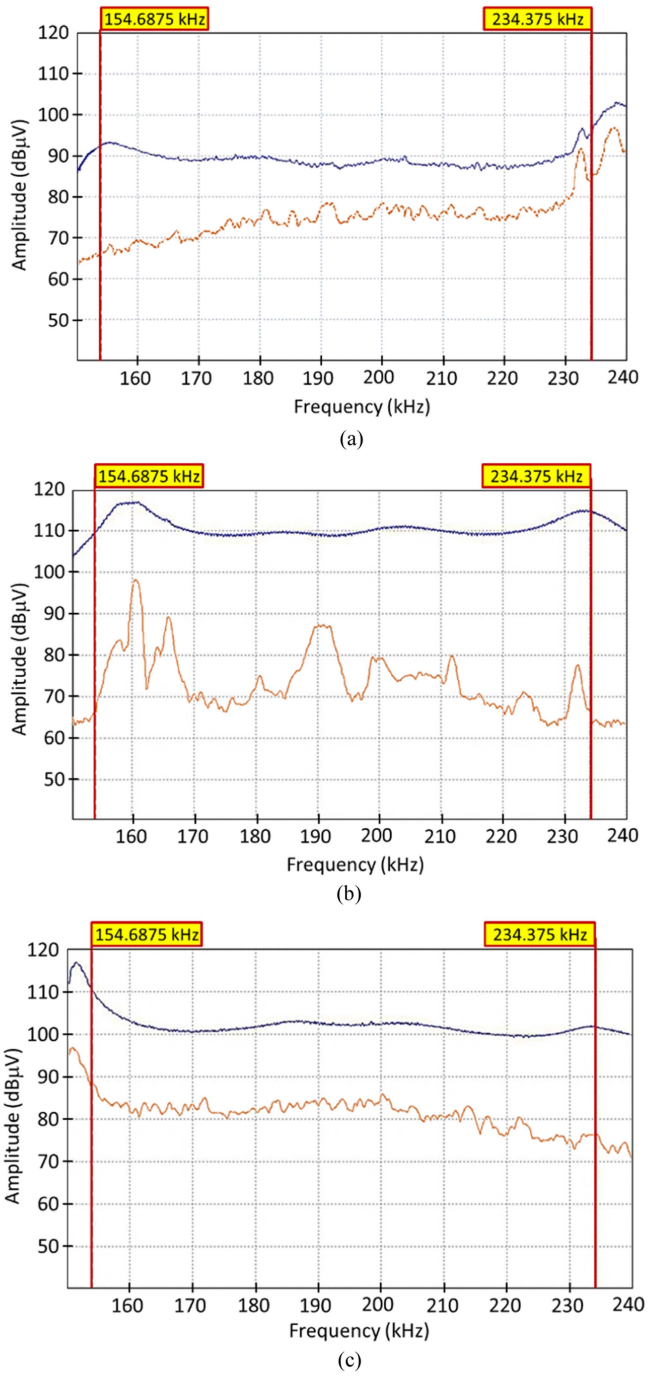

Fig. 19. Frequency response (blue plot) and noise (orange plot) measurements. Tests with 18 sub-carriers (first sub-band, centered in 194 kHz). (a) SC-based coupling without Lbd and filter; (b) SC-based coupling with Lbd and filter. (c) VDS-based coupling.

1.1 km cable and in the presence of mains voltage. In comparison with laboratory tests, measurements results showed heightened signal attenuation and noise levels. Despite these challenges, the system demonstrated remarkable adaptability to the impedances of secondary substations. The resonant system proved effective in capturing and amplifying the modulated signal, showing the system's overall versatility.

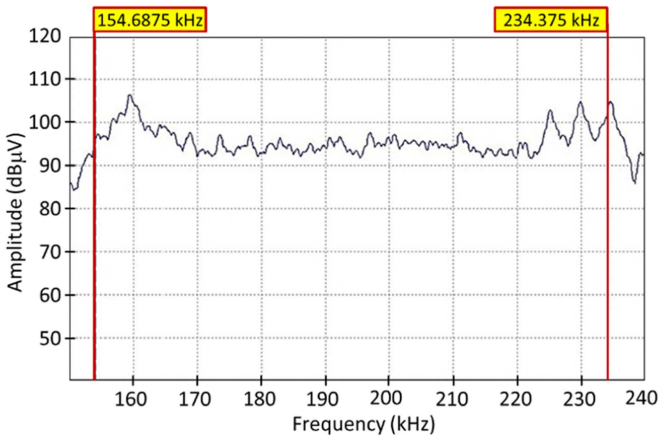

Fig. 20. Transmission tests. 18 sub-carriers OFDM 8-PSK modulated signal (first sub-band, centered in 194 kHz). Received OFDM modulated signals for the first sub-band. SC-based coupling, with Lbd and filter.

IV. Laboratory Tests

Laboratory tests were carried out to verify the SC-based coupler performances. The test bench is shown in Fig. 18.

Laboratory measurements with SCs were not made in the presence of power, i.e., the C connector of the SC in Fig. 1 was left open. RX and TX circuits described in Section III were included in an interface card prototype. A switch controlled by a transceiver output is used to select the TX or RX circuit. The interface card was connected to SC A–B terminals; B terminal was connected to earth by means of the inductance L_{BD}. Through these terminals it is possible to inject the signal on the MV cable. Two commercial SCs (Elcon Megarad ELCOSPINA TCI 20C4) were connected at the end of a MV cable (about 10 m long).

Through the resonant system, the modulated signal can be effectively captured and amplified, showcasing the system's high versatility. System performances were evaluated by measuring the following parameters:

- Received voltage level,
- Success rate,
- SNR.

In detail, received voltage level was measured using a Rohde & Schwarz RTO 1044 oscilloscope and a high voltage probe Tektronix P5200A, which was connected at transceiver input terminals. Success rate was evaluated as the ratio between the correctly received packets over all transmitted packets. SNR was directly measured by the transceiver.

Two commercial transceivers (STMicroelectronics EVALKITST8500-1) were used to transmit and receive PLC modulated signals. They can transmit and receive OFDM signals, compliant with ITU-T G.9903 (G3-PLC) standard, in the FCC above CENELEC frequency range (154.6875 kHz - 487.500 kHz). Moreover, the tone mask can be varied through a Graphical User Interface (GUI), by choosing among 4 sub-bands of 80 kHz with 18 sub-carriers or 2 sub-bands of 160 kHz with 36 sub-carriers. The 80 kHz sub-bands are centered at the following frequencies, i.e., 194 kHz, 279 kHz, 363 kHz and 447 kHz while the 160 kHz sub-bands are centered

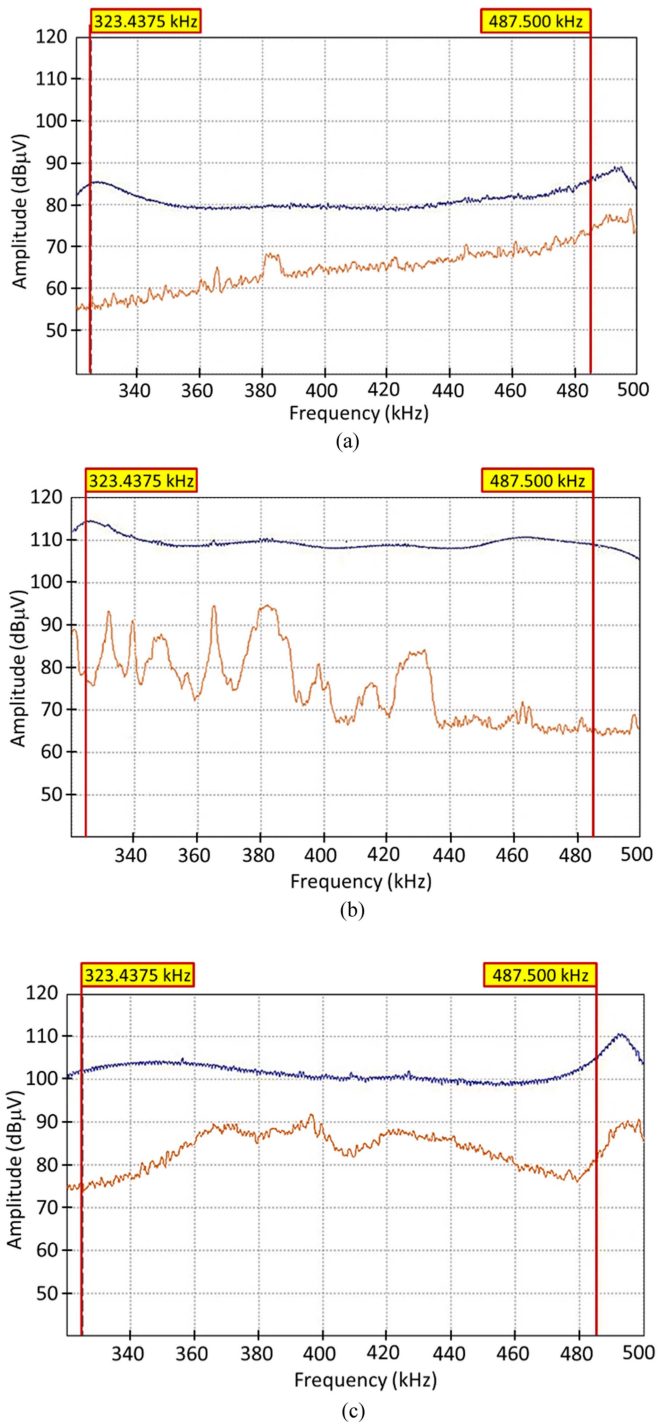

Fig. 21. Frequency response (blue plot) and noise (orange plot) measurements. Tests with 36 sub-carriers (second sub-band, centered in 405 kHz). (a) SC-based coupling without Lbd and filter; (b) SC-based coupling with Lbd and filter. (c) VDS-based coupling.

at the frequencies of 237 kHz and 405 kHz. EVALKITST8500-1 GUI were used to set transmission parameters and to measure success rate.

The tests were divided into two parts. Firstly, the system was tuned by sending a frequency sweep on the transmission side and by adjusting the parameters both in reception and transmission, so to obtain a flat band in the desired frequency

TABLE I
LABORATORY TESTS USING OFDM MODULATION WITH 18 SUB-CARRIERS – SC-BASED COUPLING

Tone Masks [kHz]	SUCCESS RATE (% – Percentage ratio between correct and transmitted pkts)								SNR[dB]
	Coherent				Differential				
	ROBO	BPSK	QPSK	8PSK	ROBO	BPSK	QPSK	8PSK	
154.6875 ÷ 234.375	100	100	100	100	100	100	100	100	20.5
239.0625 ÷318.75	100	100	100	99	100	100	100	100	30.2
323.4375 ÷ 403.125	100	100	99	100	100	100	100	99	27.6
407.8125 ÷ 487.500	100	100	100	99	100	100	100	99	30.5

TABLE II
LABORATORY TESTS USING OFDM MODULATION WITH 36 SUB-CARRIERS– SC-BASED COUPLING

Tone Masks [kHz]	SUCCESS RATE (% – Percentage ratio between correct and transmitted pkts)								SNR[dB]
	Coherent				Differential				
	ROBO	BPSK	QPSK	8PSK	ROBO	BPSK	QPSK	8PSK	
154.6875 ÷ 318.75	100	100	92	0	100	100	89	0	15.5
323.4375 ÷ 487.500	100	98	100	100	100	99	100	99	27.6

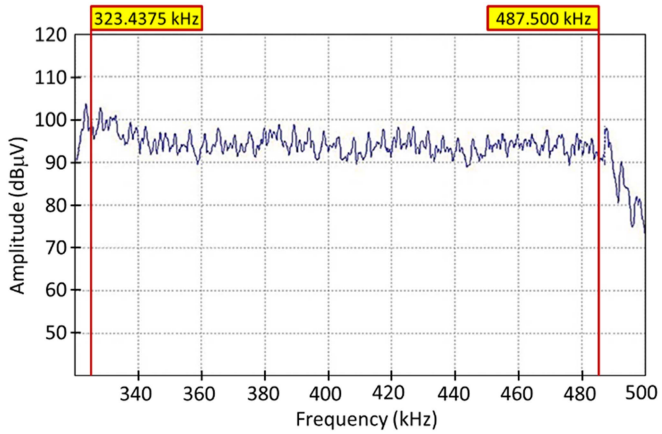

Fig. 22. Transmission tests. 36 sub-carriers OFDM 8-PSK modulated signal (first sub-band, centered in 405 kHz). Received OFDM modulated signals for the first sub-band. SC-based coupling, with Lbd and filter.

ranges. The frequency response was obtained by generating a sweep signal of 1 Vpp with a waveform generator; both TX and RX inductors and the filter resistances were tuned to obtain a flat band in the frequency range of interest. Secondly, transmission tests were performed by injecting an OFDM signal. The two EVALKITST8500-1 were used to modulate and to demodulate the OFDM signal.

A. OFDM Results With 18 Sub-Carriers

The first tests were carried out for the case of 4 sub-bands of 80 kHz. The frequency sweep tests were performed, centered at each sub-band central frequency, with a span of 100 kHz and a sweep time of 150 ms. These tests were used to set the adjustable parameters (inductances and filter resistors), so to have a flat frequency response. Noise measurements were also carried out, in the same test conditions. As an example, the results for the sub-band 154.6875 ÷ 234.375 kHz are reported in Fig. 19(a), (b), and (c), for the case with SC-based coupling without Lbd and filter, SC-based coupling with Lbd and filter and VDS-based coupling, respectively. The VDS results have been obtained on the same test bench used for the SC results by replacing the SC with the VDS.

As can be seen, a flat frequency response was obtained with a maximum variation of about 10 dBµV. SNR get worse when Lbd is not connected, due to low signal level. On the contrary, when Lbd and filter are used, the SNR becomes better than that obtained with the previous VDS-based solution. Similar results were obtained also for the higher sub-bands.

After the parameters tuning, transmission tests were performed. The spectrum of the received OFDM signal is shown in Fig. 20, for the case with SC-based coupling with Lbd and filter. It shows an average voltage of about 100 dBµV and a frequency ripple less than 10 dBµV.

The results were comparable to those obtained with the VDS-based coupling solution. All transmission test results are summarized in Table I (18 sub-carriers and SC-based coupling with Lbd and filter). They were obtained using OFDM signals with all modulations available in EVALKITST8500-1. In all cases, the success rate was higher than 99%.

B. OFDM Results With 36 Sub-Carriers

Further tests were performed to verify the possibility to extend the frequency band up to 160 kHz. As for the previous case, frequency sweep tests were performed to tune the adjustable parameters and to obtain a flat frequency response around the sub-band center frequencies, i.e., 237 kHz and 405 kHz. Noise measurements were also carried out. As an example, in Fig. 21(a), (b), and (c) the results are shown for 405 kHz centered frequency, for the case with SC-based coupling without Lbd and filter, SC-based coupling with Lbd and filter and VDS-based coupling, respectively. As for the 80 kHz band results, a flat frequency response was obtained. The best results of frequency response were obtained in the case of SC-based coupling with Lbd and filter.

The communication tests results for the second sub-carrier band (323.4375÷487.500 kHz, SC-based coupling with Lbd and filter) are shown in Fig. 22. Also in this case, they were

comparable to those previously obtained with the VDS-based coupling solution.

A summary of results with different OFDM modulations are reported in Table II for both sub-carrier bands (154.6875÷318.75 kHz and 323.4375÷487.500 kHz). Both coherent and differential BPSK and QPSK modulations between 154.6875÷318.75 kHz had a high success rate with an SNR level of 15.5 dB. In the range 323.4375÷487.500 kHz, on the other hand, all modulations had a high success rate large SNR of about 25 dB. On the other hand, with the 8-PSK modulation no packets were correctly received because of its low noise margin. This increase the probability of an overlap of two subsequent symbols, leading to a corruption of the corrupting the information which cannot be demodulated anymore.

V. Conclusion

In this paper, a PLC coupling system was designed and characterized, based on the use of capacitive dividers embedded in commercial cable separable connector (SC) of MV cables heads. The aim of this coupler is to transmit PLC signal in accordance with IEEE STD 1901.2-2013 and to evaluate the success rate with different modulations and center frequencies; in detail the attention was focused on OFDM modulation in the FCC above CENELEC frequency band, i.e., between 154.6875 and 487.500 kHz. Moreover, two cases were analyzed, i.e., OFDM signals with 18 or 36 sub-carriers.

To design the coupler, the SCs were characterized by using impedance measurement at all terminals. The measured impedances had a capacitive behavior. Thus, a circuital model was obtained. It was helpful to design an ad-hoc electronic board with adjustable parameters. The board was appropriately to maximize performance in MV. The designed interface board was built and tested in the laboratory. A special test bench was set up to evaluate the performance of the system. First, frequency response tests were performed. They were used to set adjustable parameters to have a flat frequency response. It was shown that it is possible to obtain a very flat frequency response in the case of signals with a bandwidth of 80 kHz. In detail, it was shown that it is possible to establish effective communication with the SC with high values of success rate while maintaining a high SNR; it was also possible to communicate with 18 subcarriers even 8-PSK type modulations in all ranges. Measurements with 36 subcarriers showed that it was possible to communicate with high success rates up to QPSK, while only at higher frequencies could 8-PSK modulated signals be received correctly. Next, communication tests were performed, and the following parameters were measured to verify transmission performance.

Next steps will involve on field test measurements, to verify the feasibility of PLC communication by means of SC solution in real distribution network. Due to the similarities between the VDS and the SC behavior, good results are expected also in on field measurements with SC.

The proposed SC based solution, together with the previous developed by the authors for VDS installed in the MV switchgears of distribution network's substations, confirm the feasibility of coupling PLC signal by means of elements already installed in MV networks thus reducing cost of installations of dedicated PLC couplers.

Acknowledgment

The authors would like to thank STMicroelectronics and Layer Electronics Srl for their scientific and technical support. The paper contents are the sole responsibility of the authors and they do not necessarily reflect either the point of view of the European Union or that of the Program Managing Authority.

References

[1] M. Fernández et al., "A new voltage probe with improved performance at the 10 kHz–500 kHz frequency range for field measurements in LV networks," *Measurement*, vol. 145, pp. 519–524, 2019.

[2] G. D'avanzo, A. Delle Femine, D. Gallo, C. Landi, and M. Luiso, "Impact of inductive current transformers on synchrophasor measurement in presence of modulations," *Measurement*, vol. 155, 2020, Art. no. 107535.

[3] S. Rinaldi et al., "Design of a time dissemination system using chirp modulation for medium voltage smart grid applications," *IEEE Trans. Instrum. Meas.*, vol. 69, no. 9, pp. 6686–6695, Sep. 2020.

[4] G. Crotti, G. D'avanzo, D. Giordano, S. P. Letizia, and M. Luiso, "Extended sindicomp: Characterizing MV voltage transformers with sine waves," *Energies*, vol. 14, 2021, Art. no. 1715.

[5] L. H. L. Rosa, C. F. M. Almeida, D. De Souza Pereira, and N. Kagan, "A systemic approach for assessment of advanced distribution automation functionalities," *IEEE Tran. Power Del.*, vol. 34, no. 5, pp. 2008–2017, Oct. 2019.

[6] D. Giustina and S. Rinaldi, "Hybrid communication network for the smart grid: Validation of a field test experience," *IEEE Trans. Power Del.*, vol. 30, no. 6, pp. 2492–2500, Dec. 2015.

[7] G. López et al., "The role of power line communications in the smart grid revisited: Applications, challenges, and research initiatives," *IEEE Access*, vol. 7, pp. 117346–117368, 2019.

[8] G. Hallak, C. Nieß, and G. Bumiller, "Accurate low access impedance measurements with separated load impedance measurements on the power-line network," *IEEE Trans. Instrum. Meas.*, vol. 67, no. 10, pp. 2282–2293, Oct. 2018.

[9] I. Fernandez et al., "Measurement system of the mean and sub-cycle LV grid access impedance from 20 kHz to 10 MHz," *IEEE Trans. Power Del.*, vol. 38, no. 3, pp. 2204–2212, Jun. 2023.

[10] G. Artale et al., "A new PLC-based smart metering architecture for medium/low voltage grids: Feasibility and experimental characterization," *Measurement*, vol. 129, pp. 479–488, 2018.

[11] M. A. O. Kharraz, D. Picard, M. Serhir, C. Lavenu, and P. Jensen, "Measurement methods of outdoor low-voltage cable characteristics for narrowband power line communication," *IEEE Trans. Power Del.*, vol. 34, no. 5, pp. 1818–1826, Oct. 2019.

[12] G. S. Lima and A. De Conti, "Narrowband PLC channel attenuation due to a multi-grounded neutral," *IEEE Trans. Power Del.*, vol. 36, no. 2, pp. 639–650, Apr. 2021.

[13] R. Lefort, R. Vauzelle, V. Courtecuisse, N. Idir, and A. M. Poussard, "Influence of the MV/LV transformer impedance on the propagation of the PLC signal in the power grid," *IEEE Trans. Power Del.*, vol. 32, no. 3, pp. 1339–1349, Jun. 2017.

[14] T. A. Papadopoulos, C. G. Kaloudas, A. I. Chrysochos, and G. K. Papagiannis, "Application of narrowband power-line communication in medium-voltage smart distribution grids," *IEEE Trans. Power Del.*, vol. 28, no. 2, pp. 981–988, Apr. 2013.

[15] L. G. da Costa, A. Queiroz, B. Adebisi, V. Costa, and M. Ribeiro, "Coupling for power line communications: A survey," *J. Commun. Inf. Syst.*, vol. 32, no. 1, Mar. 2017, Art. no. 25462.

[16] *Live Working - Voltage Detectors - Part 1: capacitive Type to be Used for Voltages Exceeding 1 kV A.C.*, Standard 61243-1, IEC, Geneva, Switzerland, 2009.

[17] *IEEE Standard for Low-Frequency (Less Than 500 kHz) Narrowband Power Line Communications For Smart Grid Applications*, IEEE Standard 1901.2, 2013.

[18] H. Cavdar and E. Karadeniz, "Measurements of impedance and attenuation at CENELEC bands for power line communications systems," *Sensors*, vol. 8, no. 12, pp. 8027–8036, Dec. 2008.

[19] P. A. J. Van Rensburg, B. P. Watkins, and S. Alahakoon, "Design of a current-transformer based inductive coupler for power-line communications," *IEEE Trans. Power Del.*, vol. 38, no. 3, pp. 1788–1798, Jun. 2023.
[20] P. A. J. Van Rensburg, M. P. Sibanda, and H. C. Ferreira, "Integrated Impedance-matching coupler for smart building and other power-line communications applications," *IEEE Trans. Power Del.*, vol. 30, no. 2, pp. 949–956, Apr. 2015.
[21] P. A. A. F. Wouters, P. C. J. M. van der Wielen, J. Veen, P. Wagenaars, and E. F. Steennis, "Effect of cable load impedance on coupling schemes for MV power line communication," *IEEE Trans. Power Del.*, vol. 20, no. 2, pp. 638–645, Apr. 2005.
[22] S. Raponi, J. H. Fernandez, A. Omri, and G. Oligeri, "Long-term noise characterization of narrowband power line communications measurements, analysis and modeling," *IEEE Trans. Power Del.*, vol. 37, no. 1, pp. 365–373, Feb. 2022.
[23] T. R. Oliveira et al., "Characterization of hybrid communication channel in indoor scenario," *J. Commun. Inf. Syst.*, vol. 31, no. 1, pp. 224–235, Nov. 2016.
[24] C. Leeb, D. Isch, and D. Cachin, "Medium voltage power line communication coupler," E.P. 2757705A1, Jul. 23, 2014.
[25] L. Lampe, A. M. Tonello, and T. G. Swart, *Power Line Communications: Principles, Standards and Applications from Multimedia to Smart Grid*, 2nd ed. Hoboken, NJ, USA: Wiley, Apr. 2016.
[26] Z. W. Swana, P. A. J. Van rensburg, and H. C. Ferreira, "Is resistive coupling feasible for the reception of power-line communications data?," in *Proc. Int. Symp. Power Line Commun. Appl.*, 2015, pp. 47–52.
[27] R. Fiorelli, A. Cataliotti, D. Di Cara, and G. Tinè, "Coupling circuit for power line communications," U.S. Patent 8896393 b2, Nov. 25, 2014.
[28] G. Artale et al., "A new low cost coupling system for power line communication in medium voltage smart grids," *IEEE Trans. Smart Grid*, vol. 9, no. 4, pp. 3324–3329, Jul. 2018.
[29] G. Artale et al., "A new low cost power line communication solution for smart grid monitoring and management," *IEEE Instrum. Meas. Mag.*, vol. 21, no. 2, pp. 29–33, Apr. 2018.
[30] *Plug-in Type Bushings Above 1 kV up to 52 kV and from 250 A to 2,50 kA for Equipment Other Than Liquid Filled Transformers*, EN Standard 50181, 2010.
[31] G. Artale et al., "A new coupling solution G3-PLC employment in MV smart grids," *Energies*, vol. 12, no. 13, 2019, Art. no. 2474.
[32] E5080a Ena Vector Network Analyzer, Data Sheet 5992-0291en, Keysight Technologies, 2020. [Online]. Available: https://www.keysight.com/it/en/assets/7018-04644/data-sheets/5992-0291.pdf
[33] Keysight 85032f Type-N 50 Calibration Kit, User's and Service Guide, Keysight Technologies, 2014. [Online]. Available: https://www.keysight.com/it/en/assets/9018-01295/user-manuals/9018-01295.pdf

Giovanni Artale (Member, IEEE) received the M.S. degree in electronic engineering and the Ph.D. degree in electronic and telecommunication engineering from the University of Palermo, Palermo, Italy, in 2010 and 2014, respectively. He is currently a Researcher with the Department of Engineering, University of Palermo. His research interests include low-frequency harmonic analysis algorithms, power line communications, and smart grids.

Antonio Cataliotti (Member, IEEE) received the M.S. and Ph.D. degrees in electrical engineering from the University of Palermo, Palermo, Italy, in 1992 and 1998, respectively. He is currently a Full Professor of electrical and electronic measurements with the Department of Engineering, University of Palermo. His research interests include power quality measurements, power line communications, and smart grids.

Valentina Cosentino (Member, IEEE) received the M.S. and Ph.D. degrees in electrical engineering from the University of Palermo, Palermo, Italy, in 2001 and 2005, respectively. She is currently an Associate Professor of electrical and electronic measurements with the Department of Engineering, University of Palermo. Her research interests include energy and power quality measurements, virtual instrumentation, measurement and communications systems for smart grids. She is currently an Associate Editor for IEEE TRANSACTIONS ON POWER DELIVERY and IEEE TRANSACTIONS ON INSTRUMENTATION AND MEASUREMENT

Dario Di Cara (Member, IEEE) received the M.S. and Ph.D. degrees in electrical engineering from the University of Palermo, Palermo, Italy, in 2005 and 2009, respectively. Since 2012, he was a Researcher with the National Research Council of Italy. His research interests include power quality measurements, current transducers characterization in non-sinusoidal conditions, power line communications, and smart grids.

Vito Ditta received the M.S. degree in electrical engineering in 2020 from the University of Palermo, Palermo, Italy, where he is currently working toward the Ph.D. degree in energy. His research interests include power quality measurements, harmonics, virtual instrumentation, microcontroller systems, and smart grids.

Salvatore Guaiana received the M.S. degree in electronics and photonics engineering and the Ph.D. degree in energy and information technologies from the University of Palermo, Palermo, Italy, in 2012 and 2019, respectively. He is currently a Research Fellow with the Institute of Marine Engineering, Italian National Research Council, Palermo. His research interests include power line communications, development of microcontroller systems, and communications protocols for smart grids applications.

Nicola Panzavecchia received the M.S. degree in computer science, the master's degree in domotics and building automation, and the Ph.D. degree in information and communication technologies from the University of Palermo, Palermo, Italy, in 2007, 2011, and 2022, respectively. Since 2007, he has been a Consultant, Developer, System Administrator, Cloud Architect. Since 2013, he has been with the Institute of Marine Engineering, the National Research Council of Italy, Palermo, firstly as a Research Fellow and since 2020 as a Researcher. He has developed software and hardware solutions in the framework of several research projects. His research interests include software development for energy management and embedded systems, smart grids, and power line communications.

Giovanni Tinè (Member, IEEE) received the M.S. degree in electronic engineering and the Ph.D. degree in electronics, computer science, and telecommunications engineering from the University of Palermo, Palermo, Italy, in 1990 and 1994, respectively. Since 2000, he has been a Researcher with the National Research Council of Italy. His main scientific interests include distributed measurement system for smart grids, power-line communication in medium and low voltage systems, electromagnetic compatibility (EMC), and intelligent electronic devices for smart grids.

Open Access funding provided by 'Università degli Studi di Palermo' within the CRUI CARE Agreement